Modular assembly of low-dimensional coordination architectures on metal surfaces

2008 J. Phys.: Condens. Matter 20 184002

(http://iopscience.iop.org/0953-8984/20/18/184002)

J. Phys.: Condens. Matter **20** (2008) 184002 (15pp) doi:10.1088/0953-8984/20/18/184002

Modular assembly of low-dimensional coordination architectures on metal surfaces

Sebastian Stepanow[1], Nian Lin[2,3] and Johannes V Barth[4,5]

[1] Centre d'Investigacions en Nanociència i Nanotecnologia (CIN2-ICN), UAB Campus, E-08193 Bellaterra, Barcelona, Spain
[2] Max-Planck-Institut für Festkörperforschung, Heisenbergstrasse 1, D-70569 Stuttgart, Germany
[3] Department of Physics, The Hong Kong University of Science and Technology, Clear Water Bay, Kowloon, Hong Kong, China
[4] Physik Department E20, Technische Universität München, James Franck Strasse, D-85748 Garching, Germany
[5] PHAS-AMPEL, UBC, 2355 East Mall, Vancouver V6T 1Z4, Canada

Received 4 September 2007, in final form 8 January 2008
Published 17 April 2008
Online at stacks.iop.org/JPhysCM/20/184002

Abstract
The engineering of highly organized molecular architectures has attracted strong interest because of its potential for novel materials and functional nanoscopic devices. An important factor in the development, integration, and exploitation of such systems is the capability to prepare them on surfaces or in nanostructured environments. Recent advances in supramolecular design on metal substrates provide atomistic insight into the underlying self-assembly processes, mainly by scanning tunneling microscopy observations. This review summarizes progress in noncovalent synthesis strategies under ultra-high vacuum conditions employing metal ions as coordination centers directing the molecular organization. The realized metallosupramolecular compounds and arrays combine the properties of their constituent metal ions and organic ligands, and present several attractive features: their redox, magnetic and spin-state transitions. The presented exemplary molecular level studies elucidate the arrangement of organic adsorbates on metal surfaces, demonstrating the interplay between intermolecular and molecule–substrate interactions that needs to be controlled for the fabrication of low-dimensional structures. The understanding of metallosupramolecular organization and metal–ligand interactions on solid surfaces is important for the control of structure and concomitant function.

(Some figures in this article are in colour only in the electronic version)

1. Introduction

The directed assembly of supramolecular compounds and arrays using discrete molecular building blocks is a topic of intense research with tremendous potential in the areas of catalysis, molecular electronics, sensor design, and optics [1]. Hence, there has been a rapid advancement in the fabrication of novel architectures making use of versatile noncovalent synthesis protocols, which are mainly solution based, resulting in the formation of diverse supermolecules, polymers and networks. Frequently the structures are thermally labile, allowing one to intentionally select the final product driven either by enthalpic or entropic forces through the judicious choice of building blocks and reaction conditions. Defect structures can often be corrected to yield a desired product by adjusting reaction times and conditions, a significant advantage over conventional covalent organic synthesis. On the other hand, the weakness of the noncovalent interactions, e.g. electrostatic intermolecular coupling and hydrogen bonding, representing the main ingredients in supramolecular chemistry, often translates into multiple reaction pathways that account for poor selectivity. Among the versatile synthesis strategies, one of the high-yielding paths is provided by coordination chemistry, exploiting the interaction of organic

ligands with metal centers. Metal–ligand bonding offers a set of directional bonds of intermediate strength that is exploited to realize distinct geometric shapes. Moreover, coordination chemistry has gathered a vast database of metal–ligand pairs with a huge variety of specific binding modes giving the possibility to program selectivity and directionality directly into the binding motif, allowing for the self-assembly of supramolecular architectures as diverse as polygonal clusters, polyhedra, cages, and grids [2]. Moreover, the synthesis of highly porous solid frameworks and coordination polymers has reached a mature level [3]. Therefore, the use of transition metal centers, or in general secondary building blocks, and coordination chemistry for directing the formation of complex structures has evolved into one of the most widely used strategies for organizing molecular building blocks into supramolecular arrays.

The definition of coordination systems is not trivial and encounters difficulties. In general a given coordination system consists of a coordinating atom (coordination center) ligated to other atoms or groups of atoms (ligands) by coordination bonds that are delocalized over all or several ligands. In particular, for transition metal compounds the spatial distribution of the d orbitals realizes the delocalization of the one-electron bonding orbitals [4]. Without going into the details of the bonding mechanism, the actual orbital overlap between the central atom and the ligands is rather low compared to covalent bonds, of the order of 10%, but the delocalization of the electrons involving partially unoccupied (anti-) bonding ligand orbitals via charge donation and backdonation effectively reduces the Coulomb repulsion energy between the electrons and results in appreciable binding. Thus, the formation of a given supramolecular shape is driven by the inherent symmetry of the coordination sites available on the metal center, which depends on the d orbital occupation. Therefore, careful consideration must be given to the preferred coordination environment of the metal to be used and the binding mode of the linkers, in particular chelating ligands. Given such a coordination environment around the metal centers, the symmetric and rigid extension of the ligand system from mono- to multitopicity will automatically lead to a grid-like 1D, 2D, or 3D coordination network with regularly arrayed metal ions. The supramolecular shape is encoded in both the metal ions and in the organic ligands and the interpretation of this information during the self-assembly process leads to a mutually acceptable structure.

The principles of using metals with predetermined coordination numbers and angles as building blocks and functional units is not only an appealing method from the point of view of synthetic chemistry. Transition metal ions incorporated in such structures do not merely act as stabilizing agent of the structures but remain accessible for the construction of more complex structures [5], including open networks that can host appropriate guest species. Furthermore, they possess multiple electronic/spin states and a related variety of redox, photochemical, and magnetic properties which can be tuned by the specific coordination environment. Thus the potential applications of these complex systems lie in the scientific fields of chemistry, biology, and materials science (e.g. catalysis, sensing and construction of various devices on the molecular level [6]). When the metal centers in the final structures are coordinatively inert (fully saturated), one encounters severe limits for applications such as size- and shape-selective metal-based catalysis or use of the metal centers to form more complex structures through further coordination. These limitations can be overcome by rather sophisticated synthetic strategies, e.g. using bulky ligands which sterically hinder the attachment of the same or other types of ligand.

Recent efforts have focused on transferring concepts from supramolecular chemistry to the fabrication of low-dimensional molecular architectures on well-defined planar substrates, where their properties are more amenable to physical investigations and solid-state applications [7, 8]. On solid surfaces, however, the bonding of the adsorbates to the surface plays a role of comparable importance with that of noncovalent bonds typical of supramolecular complexes, that moreover needs to be balanced with respect to the energy barriers for translational and rotational motions of the adsorbed species [9]. Thus, one demands the development of a conceptual framework of using the surface to assist in guiding the self-assembly process, i.e. to address the positioning of molecules with surface-adapted functional units. Such a scheme is similarly of interest for the deposition of pre-assembled entities. Moreover, the surface plays an important role regarding the functional properties of the low-dimensional coordination systems it supports. In particular the properties of transition metal ions embedded in the organic layer can be affected by the intricate interplay between the present interactions, e.g. the hybridization of the metal d-states with substrate electrons can effectively screen their magnetic moments [10, 11]. The balance between metal–ligand, intermolecular, and surface interactions assumes therefore a critical role in determining the chemical and electronic properties of supramolecular layers.

The work on the formation of functional supramolecular architectures on surfaces containing metal centers can be divided into two approaches. On the one hand the molecular building blocks themselves contain a metal coordination center and the whole entity is brought to the surface where the metal ions are not involved in the linkage of the molecules. Such studies are often performed in solution (see [12], and references therein), as will be discussed in full detail elsewhere. In contrast to the situation of liquid–solid interfaces studies, in vacuum conditions it is frequently difficult to evaporate complexes stabilized by coordination interactions on surfaces due to thermal decomposition [13]—the development of more advanced techniques can help to circumvent such obstacles [14].

A special situation is encountered with metal–porphyrin or metal–phthalocyanine molecules that can be either deposited by sublimation in ultra-high vacuum conditions or in solution environments (note that for these macrocyclic compounds free-base species exist, i.e. the metal centers are not required *per se* as construction units). The building of supramolecular structures which incorporate porphyrin subunits is of great interest to many research groups. The rich photochemistry and redox properties (for example photoinduced electron

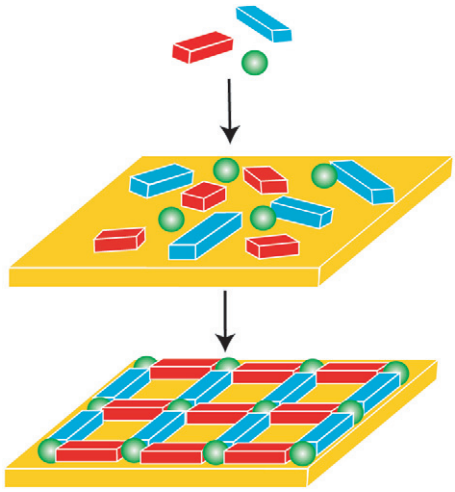

Scheme 1. Metallosupramolecular assembly of metal centers (spheres) and molecular linkers (bricks) coadsorbed on a surface.

transfer, luminescence, and light harvesting) of porphyrins have driven this interest. Porphyrins have a rich coordination chemistry that allows the inclusion of many different metal centers within the ring and at the periphery. It serves in many respects as a model system since it constitutes a low-coordination complex. Recent STM studies report on the organization of metal coordinated or pristine porphyrins as well as phthalocyanines on various metal surfaces. In particular chemically modified molecules where additional functional groups have been attached to the outer carbon atoms, e.g. pyridyl or other bulky groups, were at the focus of investigation. These additional exodentate ligands play a similar role in the determination of the adlayer structure as the functional backbone and can be used to effectively control the arrangement of the functional molecule on the surface. These systems have also been studied for their complexation chemistry directly taking place at the surface. Upon exposure to transition metal atoms selective complexation of the porphyrin macrocycle occurs leaving the template structure preserved [15, 16]. Although the complexation reaction is not involved in the formation of the adlayer structure the controlled metallization of adsorbed porphyrins provides a novel route toward high-purity metalloporphyrin architectures and patterned surfaces. Many aspects of the studies of metal–porphyrin or metal–phthalocyanine adlayer systems have been discussed previously (see [15, 17–19], and references therein) and are excluded in this review. We focus here on metal-directed organization of molecular nanostructures conducted *in vacuo*.

The assembly of metallosupramolecular architectures can be directly conducted at surfaces following the deposition of the components, i.e. organic linkers and metal atoms as illustrated in scheme 1. For the realization of low-dimensional coordination systems one has to be careful about the different mobility characteristics of the adsorbates, i.e. organic molecules and metal atoms, which can differ by several orders of magnitudes [9]. Apart from the relatively weak lateral interactions between the adsorbates there can be strong and irreversible interactions with the surface, e.g. surface alloying

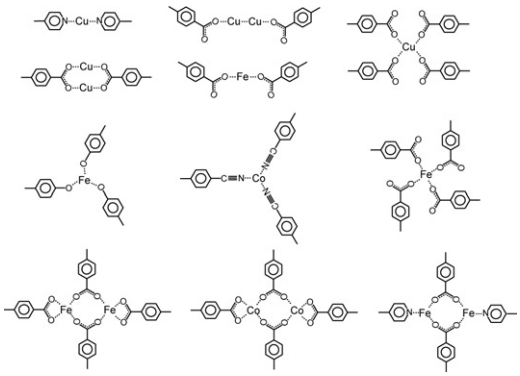

Scheme 2. Library of coordination motifs explored in surface-confined metal-ligand systems.

of metal adatoms or chemical reactions of the ligands altering their chemical state. The point of interest for their potential functional properties in the 2D metal–organic architectures is the common feature of (coordinatively unsaturated) metal centers [20]. Scanning tunneling microscopy (STM) studies of organic building blocks adsorbed on metal surfaces have shown that supramolecular ordering is governed by the competition of intermolecular hydrogen and dipolar bonds with quasiepitaxial physisorption links with the substrate. As a consequence of the components' surface confinement, the reduction to 2D is frequently accompanied by unsaturated coordination sites, which opens the way to realize novel compounds and study unsaturated yet unknown systems. Thus, the choice of donor atoms, bridging groups, paramagnetic metal ions, and systematic synthetic design strategies might render these systems ideal for designing receptor sites with tailorable molecular recognition properties and catalysts with tunable reactivities.

2. Metal–ligand interactions at vacuum–solid interfaces

In the following we provide a status report regarding the modular assembly of metal–organic compounds, polymers and networks using molecular linkers with aromatic backbones enforcing a flat adsorption configuration, i.e. with the linkers' π-systems parallel to the surface plane. The functional endgroups include carboxylate, pyridine, hydroxyl, and carbonitrile. In particular carboxylates represent a versatile class of building blocks to engineer robust 3D metal–organic frameworks or functional coordination polymers. One can similarly use metal–carboxylate coupling schemes on appropriate substrates to tailor coordination architectures in 2D. A series of systematic investigations demonstrated the construction of mononuclear metal–carboxylate clusters, polymeric coordination chains, and fully reticulated networks based on polyfunctional exodentate benzoic acid species. These findings give insight into the principles underlying the complexation of organic ligands and transition metal centers on surfaces and illustrate their potential for rational 2D metallosupramolecular engineering. Scheme 2 shows the coordination modes that have been explored so far, and

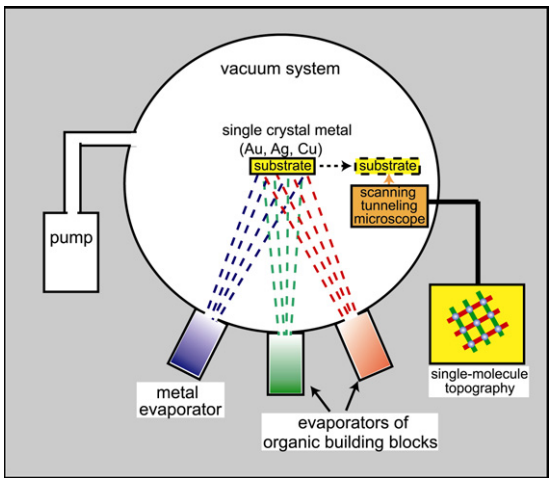

Scheme 3. Illustration of a typical experimental setup for the synthesis and subsequent STM analysis of metallosupramolecular structures at surfaces.

we shall elucidate how the intricate interplay between the driving forces in the self-assembly process leads to specific arrangements.

A typical experimental setup is sketched in scheme 3. The organic layers are generally deposited on the atomically clean surfaces by sublimation of the molecular linkers usually present in high-purity powder form. The temperature of the substrate is controllably varied from cryogenic conditions (∼10 K) to elevated temperatures (∼500 K) in order to achieve thermodynamically metastable or equilibrated products. In the surface-assembled systems the coordination centers are evaporated using electron beam or resistive heating sources. The assembly conditions are set by the substrate temperature, evaporation rate or sequence, and surface concentrations of the adsorbates.

The direct assembly of low-dimensional coordination structures starting from molecular ligands and metal atoms at vacuum–solid surfaces has been studied extensively, and to date has generated a wide range of metal–organic compounds and networks. The first evidence of lateral metal–ligand bonding in molecular systems at vacuum–solid interfaces was found for low-coverage benzoic acid adlayers on Cu(110) [21]. The proposed model contained two Cu adatoms bridging two opposing benzoate molecules. In this study it was concluded that the Cu adatoms play a specific role in the adsorption geometry of the molecules, where the π-interaction of the aromatic backbone favors a flat geometry and the carboxylate group an upright configuration. The necessary deprotonation of the acid group is thermally activated on the Cu surface. The reaction is partially accompanied with the formation of upright species. The same mechanism for the formation of molecular pairs at elevated temperatures (425 K) was proposed for 4-[*trans*-2-(pyrid-4-ylvinyl)]benzoic acid (PVBA) adsorbed on Cu(111) (see figure 1(a)) [8]. The Cu adatoms are provided by continuous evaporation/condensation from the steps of the surface [22]. The rate of detachment from the kink sites on the terraces on the Cu(111) surface is lower than on Cu(110), which is the reason for the requirements of thermal activation for complex formation in the case of PVBA compared to the benzoate structures mentioned above. Note that on the less reactive Ag(110) substrate no similar compounds evolve; however, there is a reshaping of the substrate steps induced by the functional carboxylate group [23].

The first unambiguous identification of metal–organic coordination complexes formed at a surface was demonstrated by the Cu–TMA (1,3,5-benzoic tricarboxylic acid) system. Two types of complexes, $Cu(TMA)_4$ and $Cu_2(TMA)_6$ were observed when TMA molecules were deposited at a Cu(100) surface (see figure 1(b)). In this system the metal centers are provided by the Cu substrate via thermally activated step evaporation. The energetics of the processes at the surfaces permit the monitoring of the metal–ligand bonding by imaging methods. For instance, the complexation reaction of clover-leaf-shaped $Cu(TMA)_4$ entities allows one to gain quantitative

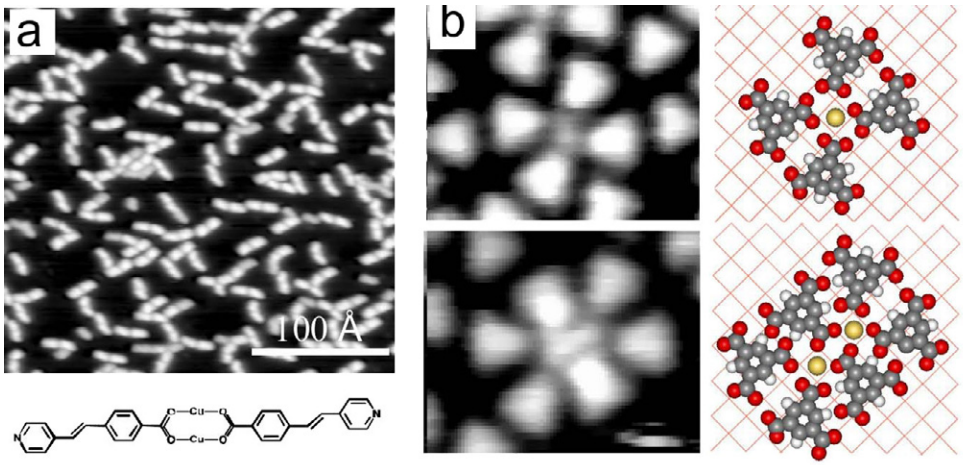

Figure 1. (a) Pairing of PVBA molecules upon deposition on Cu(111) at elevated temperatures (adsorption at 425 K, imaged at 77 K). The corresponding model shows the copper–carboxylate bonding with a head-to-head coupling of two PVBA molecules. (b) STM topographs and corresponding models of Cu–TMA complexes spontaneously assembling on Cu(100) at 300 K. The molecules' triangular shape reflects a flat-lying adsorption geometry. The upper panel shows a clover-leaf-shaped arrangement of four TMA molecules with a central Cu adatom protrusion. The lower panel depicts a STM image and model of the Cu_2TMA_6 coordination compound with four unidentate and two *syn, syn* coordination bonds. Adapted from [8] (a); and [24] (b).

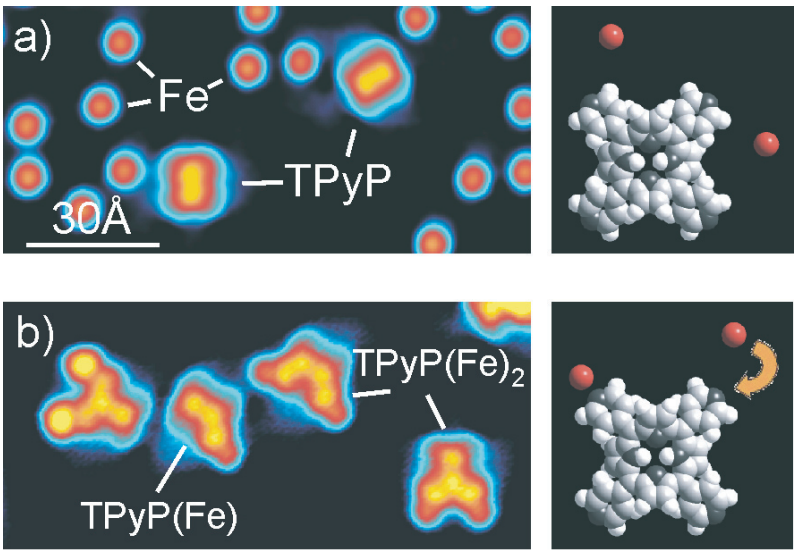

Figure 2. Selective attachment of Fe adatoms to the pyridyl groups of TPyP (images are of identical size). The porphyrin species is immobile following deposition at 300 K. (a) Upon co-deposition of Fe at very low temperatures ($T = 8$ K) there is a random distribution of Fe monomers. They become mobile at $T = 15$ K and are irreversibly attached to the porphyrins' pyridyl ligands (b). Two main steps of this experiment are schematically illustrated in the column on the right. Adapted from [19].

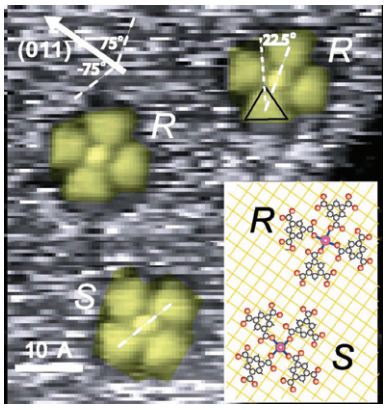

Figure 3. High-resolution image showing the two $FeTMA_4$ stereoisomers on the Cu(100) surface, labeled *R* and *S*, representing mirror-symmetric species with respect to the [011] substrate direction. The corresponding model depicts a unidentate coordination of the carboxylate ligands to the central Fe atom (placed on the hollow site) with a bond length of about 2 Å (solid lines). The corresponding rotation of the carbon backbone is strictly correlated for all TMA molecules in a given complex. The resulting symmetry break accounts for the chirality of the complexes. Adapted from [28].

information about the formation, energetics, and dynamics of individual complexes on Cu(100) [24]. The association and dissociation reactions take place in the course of tens of seconds and can readily be followed by STM imaging. It indicates that under the employed conditions the thermal motions are sufficient to dissociate this particular metal–ligand bond. The lifetime of the complexes increases dramatically when stabilized by surroundings that are either other molecules or surface step edges. Besides participating in complexation, the Cu adatoms are simultaneously potential agents for deprotonation of the carboxylic moieties engaged in the complexation reaction [25]. That is, at low temperatures where the deprotonation reaction is inhibited stable hydrogen bonded networks are observed, whereas at elevated temperatures metal–organic arrangements evolve by the catalytic activity of the substrate [26]. And as a proof of concept it was shown that TMA molecules adsorbed on a Ag(111) surface do not undergo the deprotonation reaction at ambient temperatures [25]. Only at elevated temperatures [27] or in the presence of Cu adatoms made available by co-deposition do the reactive carboxylate linkers evolve.

A direct illustration of the capture of transition metal centers by the terminal pyridyl groups of a surface-anchored porphyrin species is provided by the experiment depicted in figure 2 [19]. The isolated tetra-pyridil-porphyrin (TPyP) molecules are immobile following adsorption on a Cu(111) substrate at 300 K. Single Fe atoms were added *in situ* at 8 K, where thermal diffusion is frozen. Figure 2(a) accordingly shows randomly distributed Fe monomers appearing as round protrusions coexisting with TPyP. In a next step the sample temperature was slightly increased to about 15 K, which allows the Fe adatoms to freely migrate on the surface while the TPyP is stationary. Subsequently, the sample was cooled down again to freeze the adatom motion. As a result Fe is selectively captured by the pyridyl groups (see figure 2(b)). Once attached the adatoms stick, whereby the modified imaging characteristics of both Fe and TPyP endgroups indicate marked chemical interaction. These findings confirm that the N-containing ligands retain their affinity towards metal centers despite the simultaneously observed conformational adaptation of the porphyrin unit, implying a non-planar orientation of pyridyl groups. These measurements visualize the impact of metal–ligand interactions and a metallosupramolecular self-assembly process in 2D, where the organic linkers are spatially

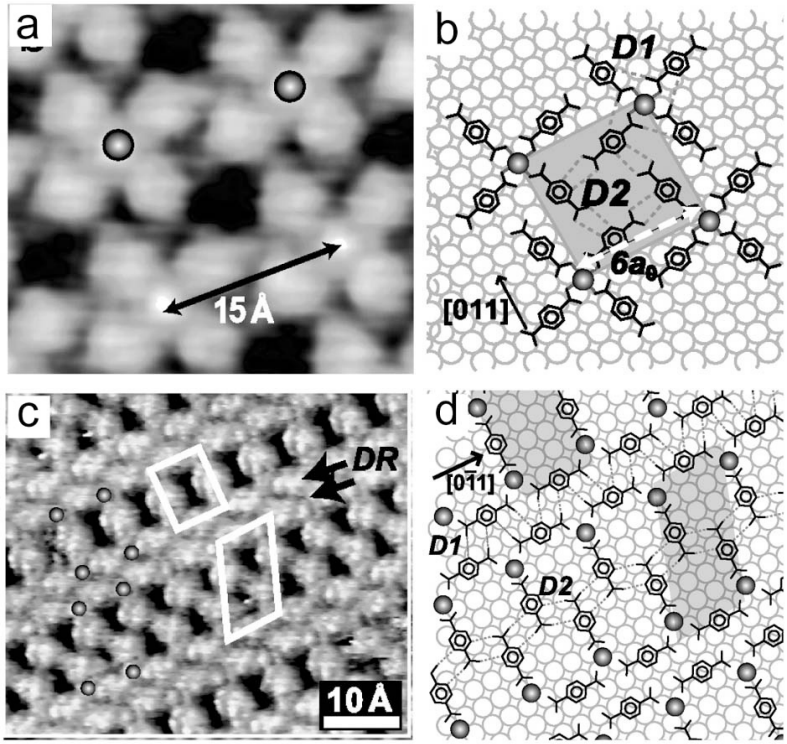

Figure 4. (a) High-resolution STM image of the Fe–TPA cloverleaf phase on Cu(100). (b) Geometrical model of the coordination structure shown in (a). Each Fe atom (gray spheres) coordinates four carboxylate ligands unidentately in a square-planar configuration. Lateral C–H···O hydrogen bonds are indicated. The distances $D1 = D2$ amount to 3.5 Å. The (15 × 15) $Å^2$ superstructure unit cell is shown as gray square. (c) STM image of the Fe–TPA ladder phase on Cu(100). The Fe atoms are marked by gray spheres and a double row by DR. (d) Geometrical model of (c). Dashed lines indicate potential C–H···O hydrogen bonds. $D1 = D2 = 3.0$ Å. Adapted from [31].

anchored. Furthermore, additional incoming Fe monomers can be trapped by the metal–ligand complex, resulting in small metal clusters pinned to the pyridyl groups of the TPyP (figure 2(b), complex on the left). In a different reaction scheme one can take advantage of the functional porphyrin macrocycle to create metalloporphyrin compounds and nanoarchitectures in 2D. Upon exposure of regular TPyP arrays self-assembled on Ag(111) to iron monomers supplied by an atomic beam, selective complexation occurs whereby the template structure is strictly preserved [15]. This expands the diversity of metalloporphyrin layers conventionally realized by evaporation of integral species, because *in situ* metallization provides a route towards novel metalloporphyrin nanoarchitectures and patterned surfaces [15, 16].

3. Zero- and one-dimensional coordination structures

The Cu–TMA complexes described above are intrinsically 0D entities because they do not organize as regular extended structures. In order to realize compounds where the supply of all constituents is controlled by the experimentalist, experiments were performed where the coordination interaction of TMA with Fe centers was probed (figure 3) [28]. The iron was co-deposited at low temperatures in order to inhibit intermixing reactions with the surface. The resulting complexes appear exclusively in the presence of Fe on the surface and are distinct from their Cu-based counterparts, notably featuring reduced bonding distances and 2D chirality. The STM observations at room temperature reveal two mirror-symmetric square-planar $Fe(TMA)_4$ complexes where the correlated attachment of the ligands defines the handedness of the entity. In contrast to the spontaneously formed Cu-carboxylate species, the Fe complexes are more compact and thermally stable at room temperature allowing the imaging of isolated $Fe(TMA)_4$ compounds. Upon annealing of the $Fe(TMA)_4$ complexes at 350 K larger entities evolve consisting of 16 TMA and 9 Fe, aggregating as a (4 × 4)-grid pattern [29]. These grid-like structures inherit the chiral nature of the central $Fe(TMA)_4$ complexes and are randomly distributed at the surface (see below). A recent study reported an even more intricate assembly scheme for a surface-supported metal–organic cluster: single nanoporous coordination structures were combined to a fractal polymeric macromolecule composed of bis-terpyridine tectons coordinating 36 Ru and 6 Fe atoms [30].

In subsequent systematic investigations it was shown that by employing the symmetric linker 1,4-benzoic dicarboxylic acid (terephthalic acid, TPA), the linear analog of TMA, one can achieve distinct regular 2D structures consisting of coordination complexes interconnected by hydrogen bonds on a Cu(100) surface in the low-Fe concentration regime [31]. The molecules form mononuclear iron complexes $Fe(TPA)_4$ where four molecules coordinate each with one carboxylate oxygen

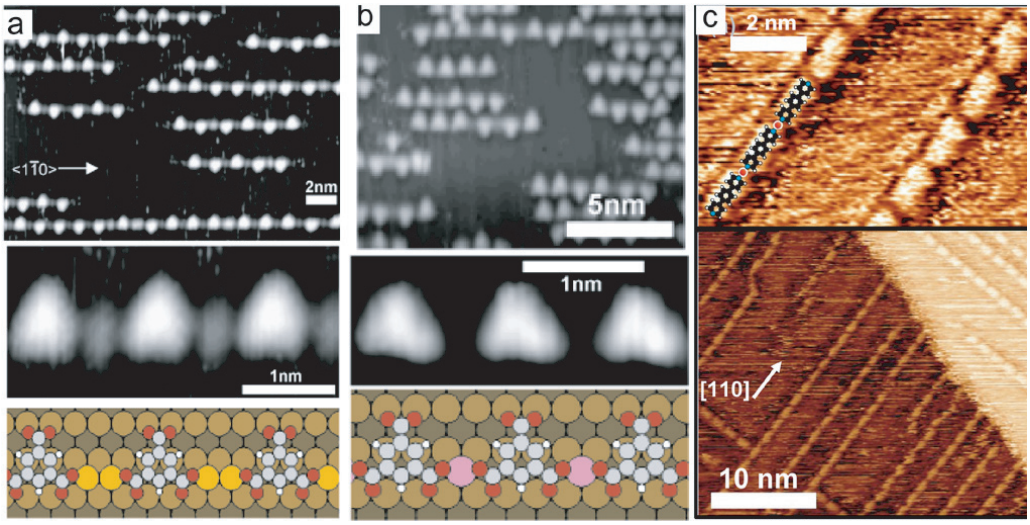

Figure 5. (a) STM data of Cu–TMA chains on Cu(110) for a TMA coverage of 0.13 ML. Below a high-resolution STM image and the corresponding model are shown. (b) STM image of the Fe–TMA chains. The high-resolution STM topograph and the corresponding model are depicted below. (c) STM images of 1,4-bis(4-pyridyl)benzene adsorbed on Cu(100) at 300 K. The structural model overlaid on the image illustrates the N–Cu–N coordination bonding. The lower STM topograph shows an overview of the chains attached to the lower side of the terrace step or running parallel on the upper side of the step. Adapted from [37] ((a), (b)) and [38] (c).

to the Fe center. The attachment of the ligands assumes two different mirror-symmetric senses of rotations around the Fe center. The individual Fe centers span a (6×6)-superstructure commensurate with the Cu(100) lattice (figure 4(a)), and this square array extends over entire substrate terraces. The high degree of long-range organization is presumably mediated by secondary intercomplex carboxylate–phenyl hydrogen bonds (see model in figure 4(b)). This rather unusual hydrogen bond has been identified in related adlayer systems [32, 33] and analyzed by theoretical means [27]. It represents a particular member of the class of ionic hydrogen bonds [34]. A domain of complexes contains only one type of handedness signaling the chiroselectivity of this intercomplex interaction. The lower symmetry derivate 1,3,4-benzoic tricarboxylic acid (trimellitic acid, TMLA) forms isomorphological structures, i.e. the remaining carboxylate side group of the TMLA molecule is not directly involved in network formation [35].

At intermediate Fe concentrations both TPA and TMLA form 1D ladder structures comprising rows of coordinated molecules along the [011] or [0$\bar{1}$1] substrate directions (figures 4(c) and (d)) [31, 36]. The ligands binding laterally to the rows either bridge two coordination centers directly or interdigitate and presumably form hydrogen bonds. The numbers of the two different links account for the Fe–ligand concentration ratio present in the self-assembled structure. Each Fe center is coordinated to three ligands in a distorted square-planar geometry. Also this structure is commensurate with the underlying substrate periodicity.

The formation of 1D structures was deliberately steered through two strategies: (1) applying anisotropic surfaces and (2) utilizing linear coordination modes. An example illustrating the first strategy is shown by depositing TMA molecules on an anisotropic Cu(110) surface [37]. Such surfaces were investigated in detail for their role in templating surface epitaxial growth. Despite the triangular arrangement of the reactive carboxylate linker moieties, which would favor 2D assemblies, the molecules form 1D systems demonstrating the strong templating effect of the substrate. The intermolecular interactions are overcome by the strong coupling to the substrate effectively controlling the 1D character (figure 5(a)). Again mobile Cu adatoms are found to link adjacent TMA molecules along the close-packed [1$\bar{1}$0] direction. Notably it was shown by DFT calculations that the misleading and tempting single protrusion observed by STM could only be reproduced in the STM simulations by a dimeric Cu center, as suggested by the geometric analysis of the structures. The intrinsic Cu–TMA linear nanostructures can be transformed into the Fe–TMA chains by preventing the formation of Cu–TMA complexes at low temperatures and following deposition of Fe. The observed chains reproduced in figure 5(b) exhibit a shorter periodicity where only single Fe ions are found as the coordination centers. Although the chain character prevails in both metal systems the different chemical nature of the coordinating metal is reflected in the composition of the structures. A recent study followed the second strategy where two linear aromatic dipyridyl linkers were investigated on the isotropic Cu(100) surface [38]. Upon deposition on the substrate held at room temperature linear chains evolve where the molecules are linked by a linear coordination motif of pyridine–Cu–pyridine (see figure 5(c)). The Cu centers are not imaged, presumably due to an electronic effect, as described in [37]. This unconventional two-fold coordination of Cu centers has not been observed in bulk coordination compounds.

4. Two-dimensional metal–organic coordination networks

Regular 2D metal–organic coordination networks (MOCNs) were realized by the direct reticulation of coordination networks in 2D. In this approach distinct levels of hierarchies

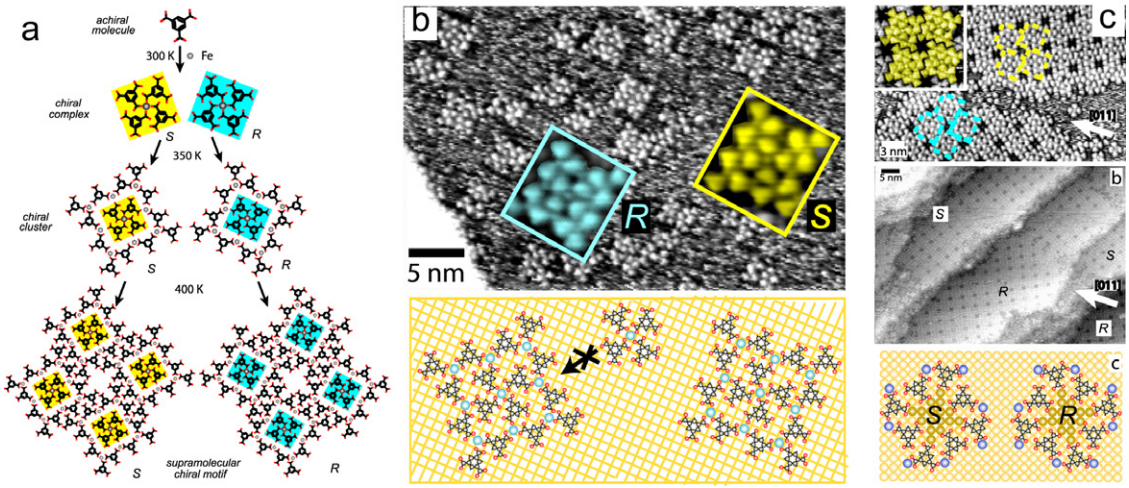

Figure 6. (a) *Aufbau* of dissymmetric supramolecular motifs mediated by hierarchical assembly of simple achiral species on Cu(100). TMA molecules and Fe atoms represent the primary units which are employed for the formation of secondary chiral complexes. The complexes are antecedents for tertiary polynuclear nanogrids which are in turn the supramolecular motifs for the assembly of homochiral nanocavity arrays. The respective mirror-symmetric configurations (labeled *S* and *R*) are indicated with a yellow and turquoise background. (b) Assembly of the tertiary stage: square-shaped polynuclear nanogrids evolve upon annealing at 350 K. The insets and model below reveal that the respective core units of the dissymmetric metal–organic motifs are related to the chiral secondary FeTMA compounds. (c) Formation of extended nanocavity arrays triggered by 400 K annealing. Two homochiral domains are assembled consisting of pure enantiomers (labeled *R* and *S*), marked by colored rectangles. The central opening of the domains, modeled in the bottom panel, is functionalized by eight surrounding carboxylate groups. Adapted from [29].

and complexity were encountered. This intriguing issue, which is abundant in biological systems, was observed in the Fe–TMA self-assembled layers on Cu(100) and is schematically reproduced in figure 6(a). As reported above, the TMA molecules and Fe adatoms initially form mononuclear chiral complexes at room temperature and these entities are antedecents for the higher level polynuclear (4 × 4)-grids at 350 K (see figure 6(b)) [29]. At the final stage, after an annealing at 400 K, the (4 × 4)-grids are interconnected by hydrogen bonds forming mesoscale networks comprising a regular arrangement of homochiral nanocavities (figure 6(c)). The only control parameter in the assembly is the temperature that limits the mobility of the secondary and tertiary entities. The control of self-assembly schemes involving hierarchical structures represents an appealing possibility for the bottom-up fabrication of complex functional materials.

With both TPA and TMLA linkers regular 2D network structures can be realized by complexation with appreciable amounts of Fe. One achieves a fully reticulated structure comprising arrays of di-iron coordination centers [31, 36]. A drawback is the existence of two equivalent isomeric structures that differ in the orientation of the Fe pairs in the network nodes, i.e. they are either equally oriented or alternate. The Fe–Fe spacing within a dimer amounts to about 4.7 Å, slightly less than twice the substrate lattice constant (2.55 Å). The coordination geometry for each Fe ion assumes a distorted square-planar geometry. Both isomeric networks reside commensurate on Cu(100) with a (6×4) and (5×5) unit cell, respectively. These structures possess cavities of well-defined size and shape exposing the underlying Cu surface (figures 7(a) and (b)) [31, 36]. Two longer analogues of TPA, 4,4′-biphenyl dicarboxylic acid (BDA) and 4,1′,4′,1″-terphenyl-1,4″-dicarboxylic acid (TDA) having two and three phenyl groups in the molecular backbone, respectively, form networks with increasing size similarly containing a di-iron center as the essential coupling motif of the carboxylate groups (figures 7(c) and (d)) [39, 40]. The dependence on the metal to ligand concentration ratio is absent for the longer molecules, and instead a coexistence of network and pristine molecular phases is observed at Fe deficiency.

The replacing of the linear C–C bridge between the two aromatic rings of the BDA molecule by an ethenyl or azo group, namely 4′,4″-*trans*-ethene-1,2-diyl-bisbenzoic acid and 4,4′-azobenzene dicarboxylic acid, significantly alters the appearance of the network structure (see figure 8). Again the di-iron coordination motif prevails. But compared to the linear polybenzene dicarboxylic linkers the network domain sizes are significantly smaller, i.e. the domains do not exceed 10 nm in size, and the structures exhibit many structural defects. Moreover the cavity sizes and shapes span a variety of geometries, and the axial orientation of the Fe pairs appears to be arbitrary. These differences can be attributed to the lower symmetry of the ligands which accounts for the presence of two enantiomers on the substrate. This lack of enantioselectivity in the self-assembled structures is in contrast to the chirally resolved hydrogen bonded pure molecular adlayers. The inclusion of both types of adsorbates in the coordination assemblies prevents the development of a perfect periodic structure that is commensurate to Cu(100). It signals the prevailing strength of the Fe–carboxylate bond in these systems [41].

The series of presented studies shows that the carboxylate functional group frequently assumes a coordination motif with a di-iron center. The carboxylate moieties are either bridging the two Fe centers or are engaged in the axial binding,

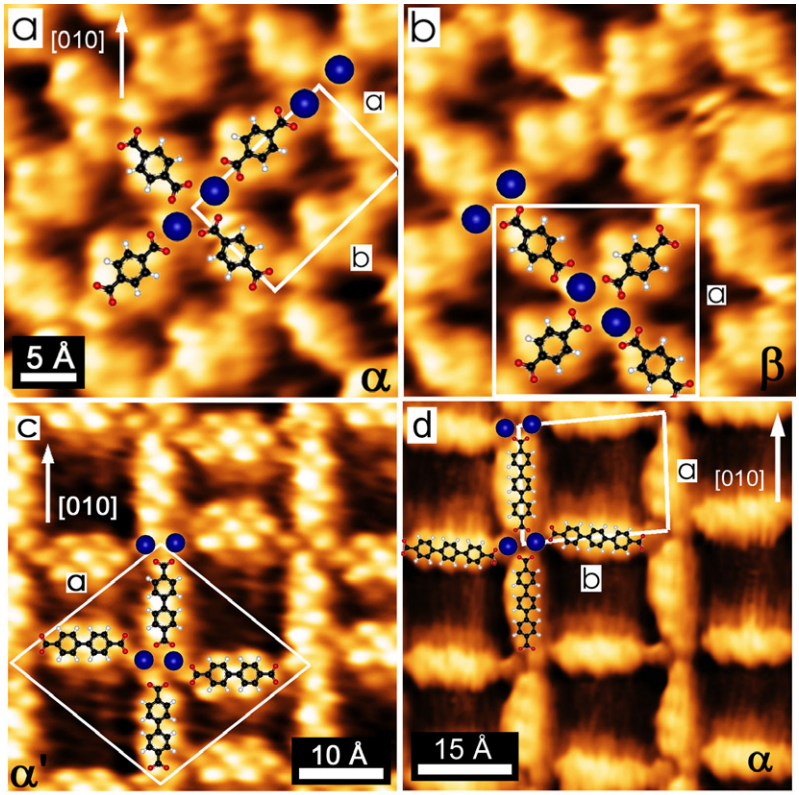

Figure 7. Fully reticulated nanoporous Fe–carboxylate networks comprising di-iron centers as a coordination motif. (a), (b) STM topographs of isomeric Fe–TPA network phases: (a) identical and (b) alternating Fe dimer arrangement. (c) High-resolution STM image of the Fe–BDA network. (d) STM image of the Fe–TDA network phase. Tentative models are superimposed on the STM images. Adapted from [40].

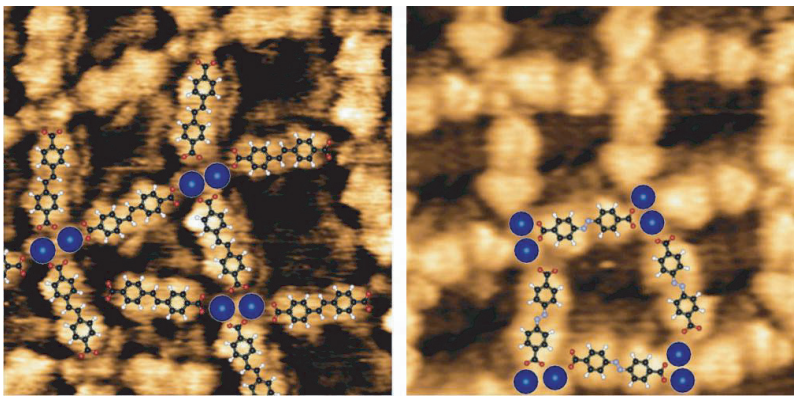

Figure 8. High-resolution STM topographs of the Fe-4′,4″ *trans*-ethene-1,2-diyl-bisbenzoic acid (left image) and Fe-4,4′-azobenzene dicarboxylic acid (right image). (Image size: 8.4 nm × 8.4 nm.) The tentative models are drawn overlaying the data. Fe is represented by spheres. Adapted from [41].

being either chelating bidentate or monodentate, which also results in the evolution of isomeric phases. By replacing the symmetric linkers to dissymmetric carboxylpyridyl ligands, namely PVBA, it was demonstrated that one can eliminate the isomeric structures (see figure 9(a)) [42]. The carboxylate moiety acts in these system solely as an equatorial linker whereas the pyridyl group binds strictly axially to the di-iron motif resulting in a three-fold coordination geometry for the metal centers. As a consequence the orientation of the di-iron centers must alternate. The realization of this structure provides the conceptual grounds that equatorial and axial ligands might be employed independently leading to more control over the design of the network structure.

Three-fold coordination motifs, leading to such complex structures as honeycomb or kagomé lattices, are scarce in 3D compounds since low-dimensional coordination modes are less frequent. In fact, low coordination numbers have only been found in complexes where the steric hindrance originating from bulky ligands results in such arrangements. At surfaces the strict 2D confinement of the ligands and metal ions imposed

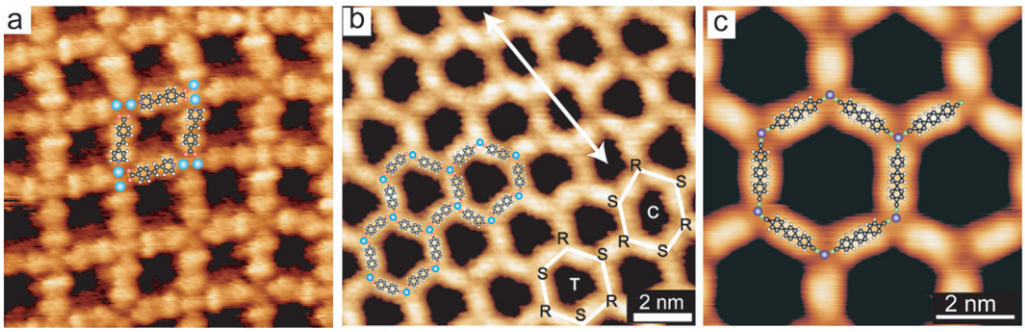

Figure 9. (a) STM topograph of the Fe–PVBA network formed on the Cu(100) substrate (8 nm × 8 nm). The asymmetric imaging of the molecule is clearly discernible. (b) STM topograph displaying the hexagonal Fe–biphenolate network assembled on Ag(111). Different cavity types are highlighted in white frames and the handedness of the coordination centers are indicated by *S* and *R*. (c) High-resolution STM image of the Co–dicarbonitrile honeycomb network assembled on Ag(111). The tentative models are superimposed over the data. Adapted from [42] (a) and [43] ((b), (c)).

by the substrate substantially influences the metal-to-ligand binding modes. In a recent study networks comprising trigonal mononuclear coordination nodes have been achieved by the Co- and Fe-directed assembly of ditopic dicarbonitrile- and hydroxyl-terminated, respectively, polybenzene linkers [43]. This is illustrated by the hexagonal superlattices realized on Cu(100) and Ag(111) surfaces, respectively, shown in figures 9(b) and (c). The occurrence of three-fold coordination motifs on substrates with different symmetries signifies that the binding motif is an intrinsic characteristic of the surface supported metal coordination and not due to templating effects. The two binding modes of the different functional groups differ with respect to the orientation of the ligand termination. The cyano-terminated ligands point directly towards the metal ion whereas the hydroxy ligands are directed slightly off center which accounts for the chirality of the binding motif. These features are intrinsic properties of the ligand system and have to be taken into account when designing coordination architectures. The results demonstrate that surface-assisted assembly can lead to unusual coordination motifs which are generally not found in conventional 3D bulk phases. These findings are attributed to the presence of the surface, where hybridization of the metal orbitals with the metal states of the substrate causes unusual redox states. In addition the preferred flat configuration of the aromatic system can stabilize such binding modes.

5. Substrate epitaxy

It is known from the well-documented inorganic epitaxy studies that substrates play a crucial role in determining the adlayer structures. Related rules have been established for organic layers [44]. Parameters like the atomic lattice constant, crystalline orientation, and atomic steps have to be taken into account. For the metal-directed organization the substrate influence is also of importance and needs to be assessed. The detailed investigation of the structural parameters of TPA, BDA, and TDA networks reveals the templating effects of the underlying substrate [40]. Besides the common feature of di-iron coordination centers in fully reticulated network domains the structures of the three molecules differ markedly in the coordination configuration and network geometries. These differences are attributed to the adsorbate–substrate coupling which plays a decisive role in the determination of the local coordination geometry. For instance the Fe–Fe spacing in the BDA structure amounts to only 3.7 Å, considerably lower than in the TPA networks. In addition the coordination configuration of BDA and TDA is different from the distorted square-planar geometry found for the Fe–TPA structure. Although the exact configuration cannot be deduced from the STM images the spatial attachment of the ligands suggests either a planar trigonal geometry or a distorted tetrahedral coordination, whereas the former has been indeed observed for hydroxy functional moieties in the same surface. Besides the local coordination geometry, the network orientation with respect to the substrate lattice is different for the three molecules. In particular the BDA and TDA molecules align along the [010] and [001] directions, where the TDA network orientation deviates slightly from the high-symmetry [010] and [001] directions implying that the structure is not precisely commensurate to the surface lattice. The influence of the substrate also has consequences for the shape of the cavities where their size reflects the length of the linkers. It is proposed that the network structures are determined by three different factors, the molecular adsorption energy, the Fe adsorption energy, and the Fe–carboxylate binding energy. The competition between the most favored molecular and metal adsorption sites and optimal coordination bonds determines the final structure. Because of the similar strength of the three forces and their subtle balance the change of the molecule backbone has dramatic consequences in the geometries.

This mechanism is expressed explicitly when the symmetry mismatch between networks and substrate atomic lattice is present [43]. On the (100) facet the hexagonal Fe–hydroxyl networks are strongly distorted, resulting in a complicated arrangement of different cavity types but preserving the honeycomb topology. This ultimately limits the domain size. In contrast to the (100) surface the networks grow continuously over entire terraces of the Ag(111) surface (see figure 10(a)). The formation of highly symmetric

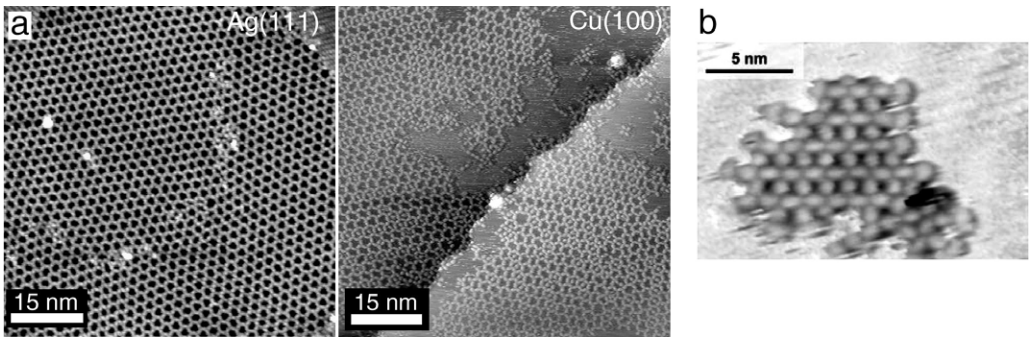

Figure 10. (a) STM overview images showing the Fe–biphenolate networks assembled on Ag(111) (left image) and Cu(100) (right image). Two large domains on the Ag(111) surface are separated by a domain boundary. Three different domains are discernible on the Cu(100) surface. The domains size is considerably smaller on Cu(100) than on Ag(111). (b) STM image of the rectangular metal–organic nanogrid of CoTPA assembled on Au(111). The structure is related to the FeTPA networks observed on the Cu(100) surface. Adapted from [43] (a) and [45] (b).

hexagons is a consequence of the matching symmetry of the underlying substrate. Moreover, the achiral coordination nodes of the cyano-network facilitate the assembly of extended domains [43]. The observed templating effects are a consequence of the preferred adsorption sites of the molecules and metal adatoms. Especially on the (100) surface the network nodes of the honeycomb structure cannot adsorb on identical sites and therefore slight displacements are caused and the network is deformed. Nevertheless the metal–ligand bonding dominates over the influence of the substrate.

In the case of rectangular Fe–TPA-or Co–TPA-coordination grids grown on the three-fold Au(111) quasihexagonal substrate [45], the mismatch of the symmetries is merely reflected in limited domain sizes (figure 10(b)). In conjunction with the DFT results (see discussion below) the formation of the network is a result of the intrinsic properties of the binding mode between the transition metal ions and the carboxylate linkers. This linkage can overcome the templating influence of the rather low corrugated Au(111) surface. The driving forces for metal–terephthalate formation on Au(111) are determined primarily by the strength of the metal–carboxylate bond.

In sharp contrast the two-fold pyridine–Cu–pyridine coordination is not strong enough to overcome the adsorbate–substrate interaction. It was shown that by adjusting the commensurability of the chain structure with the substrate the stability and structure of the chains is strongly affected, i.e. the epitaxial agreement of the molecular structure with the substrate lattice has profound effects on the growth kinetics and stability of the structures. The discussion of the commensurability of the structures in [38] as well as the dynamics of chain formation highlights once again the importance of the adsorbate–substrate interaction and its implication for the construction of such low-dimensional architectures.

6. Chemical, electronic, and magnetic analysis

While the morphology and epitaxy of ultra-thin and submonolayer molecular films have been extensively studied by STM, the characterization of the physical properties, e.g. oxidation states of metal centers and coordination geometry, of such layers is just beginning. Because of the submonolayer coverage such measurements require extremely sensitive experimental techniques, mostly offered by synchrotron radiation based methods. X-ray photoemission spectroscopy measurements for the Fe–TPA system provide direct evidences that carboxylic functions are deprotonated resulting in reactive carboxylates [32]. In a complementary x-ray absorption spectroscopy experiment for the Fe–TPA mono-iron arrays it was confirmed that indeed true coordination bonds form between Fe and carboxylate ligands, i.e. the initial metallic state of the Fe adatom on the Cu(100) surface assumes a more atomic character upon engagement in the coordination bonds [46]. This is corroborated by the vertical lift up of the Fe centers found in the DFT analysis [47]. Partial uncoupling of the Fe metallic bond with the substrate leads to effective control of the magnitude of the spin and orbital moment, as well as in-plane, out-of-plane magnetic anisotropy via modifications of the ligand field [48].

7. Theoretical analysis by DFT calculations

Theoretical analysis of metal–organic complexes in contact with solid metal substrates has been addressed by *ab initio* calculations based on density functional theory (DFT). The reported results for Fe/Co–TPA di-iron grids [45, 47], Fe–TMA chains [37], as well as isolated adsorbed porphyrins on Au surfaces [10, 18, 49] reveal the interplay of the interactions involved between ligands and metal ions as well as adsorbates and substrate in the determination of the electronic and magnetic properties of the metal centers. The results for the systems presented here have been obtained by calculations performed with the exchange and correlation energy functional expressed in the generalized gradient approximation. It was found that the molecules are rather flat on the surfaces with their carboxylate groups bending towards the surface, with the oxygen atoms residing on the top position of the Cu surface. That signifies the strong interaction of the carboxylate groups with the substrate, which has been suggested by the earlier STM findings and accounts for the strong templating effects.

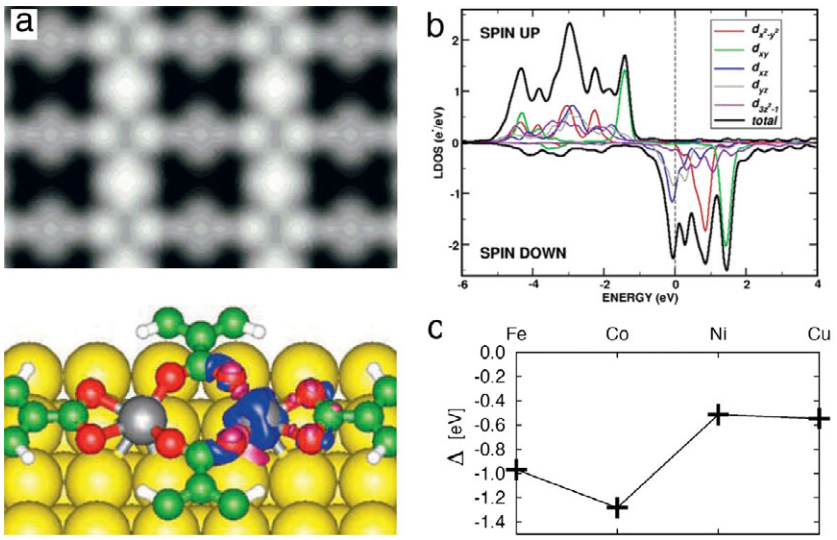

Figure 11. (a) STM image simulation showing contours of constant LDOS at the sample Fermi level derived from the DFT modeled Fe–diterephthalate grids on Cu(100). The graph below shows a perspective view of the di-iron unit. The Fe charge rearrangement contour levels indicated on the right, drawn with respect to a removed iron atom, are $\pm 0.004e^{-}$ Å^{-3}, whereby the increased (bright) and decreased (dark) electron density is indicated, respectively. (b) Spin polarization of Fe centers as evidenced in the projected density of electronic states on the Fe atomic d-states. (c) Driving force Δ for metal–carboxylate formation on Au(111) as a function of different transition metal species. Adapted from [47] ((a), (b)) and [45] (c).

Besides the elucidation of the adsorbate structure of the M–TMA chains DFT calculations give also insight into the electronic structure of the coordination centers, in particular the spin states [37]. It was found that the projected density of states displays an appreciable splitting between the majority and minority spin electronic d-states. Moreover, the spin polarization of 3.3 μ_B is comparable to the polarization of an isolated Fe adatom (3.2 μ_B). It was inferred that the coordination to the carboxylate groups does not affect the electron localization at the coordination center, i.e. does not quench the spin magnetic moment.

For the di-iron FeTPA system DFT calculations reproduce the main features appearing in the STM data (see figure 11(a)) and provide an atomistic description of the respective electronic and geometrical structure [47]. The corresponding model in figure 11(a) shows a close-up view of the carboxylate-bridged di-iron center. DFT indicates Fe–O bond lengths of 2.01 Å (equatorial) and 2.24 Å (axial), respectively, close to values in 3D Fe–carboxylates. A further striking consequence of the strong lateral Fe–carboxylate coupling is the modified Fe–substrate bonding distance upon the embedding of the Fe centers in the metal–organic array: compared with isolated Fe adatoms in a fourfold hollow position, those in the Fe–TPA grid are vertically lifted by 0.6 Å and in addition the Fe atoms are laterally displaced from the high-symmetry substrate positions (Fe–Fe spacing of 4.4 Å). Comparative calculations for the freestanding isostructural 2D Fe–TPA layer signal that the properties of the unsupported metal–organic array are close to those of the adsorbed grid; that is, the Cu(100) square atomic lattice represents an excellent template. The strong hybridization between the Fe and Cu states prevents a conclusive analysis of the Fe oxidation state. Nevertheless, also in this system there is a marked splitting between the spin majority and minority states as observed in the projected density of states presented in figure 11(b). The resulting spin polarization accounts for strongly magnetized Fe centers bearing a magnetic moment of 3.4 μ_B, coming close to the spin moment in the mononuclear Fe–TMA chains grown on the Cu(110) substrate. The magnetic coupling between the centers is present but their nature (ferro- or antiferromagnetic coupling) could not conclusively be determined.

The dependence of the metal–ligand formation on the nature of the coordination center was addressed by DFT calculations for the M–TPA system on Au(111), where M = Fe, Co, Ni, Cu [45]. The energetics of the process involve the chemisorption energy of the adsorbed M–TPA complex, the individual adsorbates, i.e. metal adatom and molecule, and the gas phase molecules/products. It was assumed that the major contribution is given by the metal–surface and metal–carboxylate interaction, whereas the molecules–surface interaction does not vary strongly with different metals bound to the molecule. The interaction energy is further divided into the binding energy in the gas phase, the adhesion energy of the metal adatom on the surface, and the cohesion energy of the bulk metal, i.e. the energy gain of a gas phase atom incorporated into an island. It was found in the study of four transition metal atoms (Fe, Co, Ni, and Cu) that the strongest binding energy in the gas phase has been determined for Co, followed by Fe and with some distance the less reactive Ni and Cu atoms. The transition metals generally have a strong tendency to form clusters and islands, so the binding energy to the carboxylate group determines the driving force for the complexation of the metals. The relatively low cohesive energy of Cu compared to the other metals makes it easily available on the surface for metal–ligand bonding although the binding energy to the carboxylate groups is rather low (figure 11(c)).

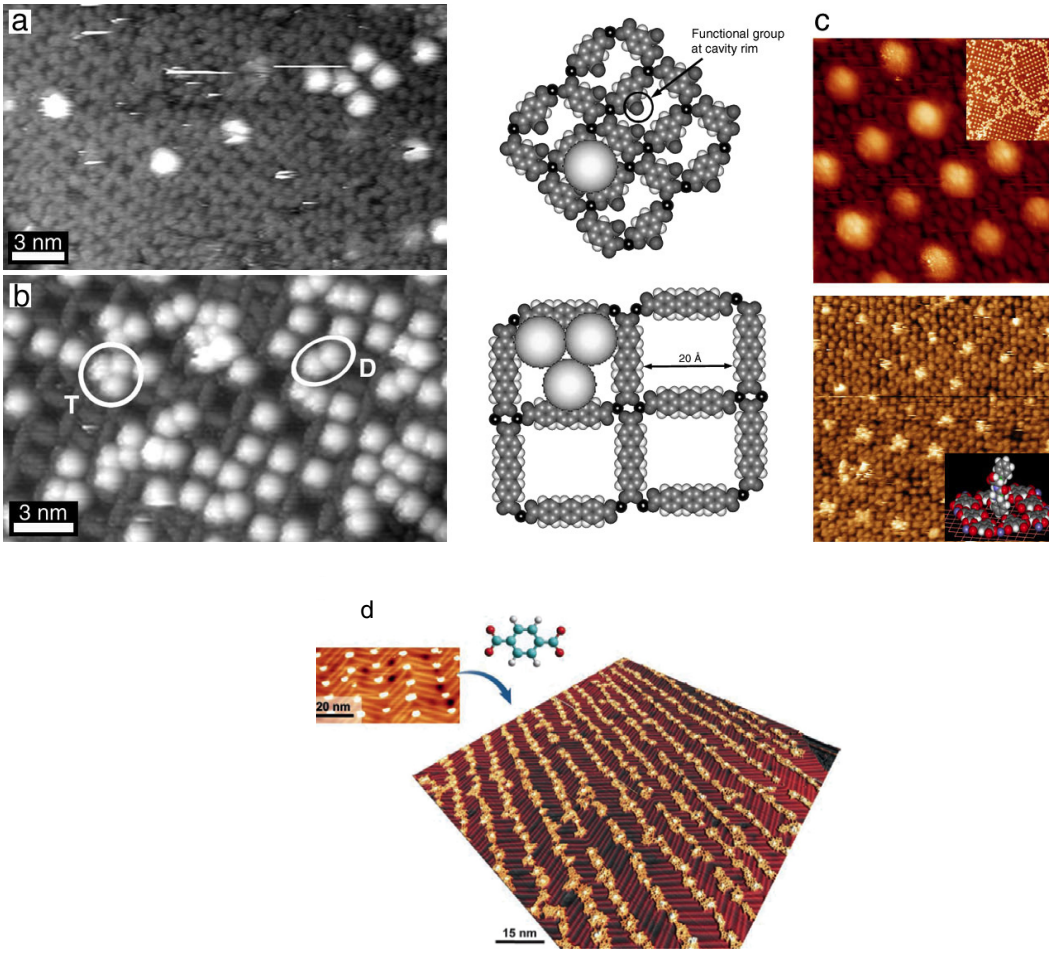

Figure 12. (a), (b) STM data and models showing the accommodation of C_{60} in nonporous (a) Fe–TMLA and (b) Fe–TDA networks. Similar to the Fe–TPA grids, Fe–TMLA networks host exclusively C_{60} monomers. The indicated functional side group strongly affects the chemical reactivity of the cavity. The mesoscale cavities in Fe–TDA networks can host C_{60} monomers, dimers (D), and trimers (T). (c) Binding of C_{60} (upper image) and diphenylalanine (lower image) in the Fe–TMA nanocavities. The apparent fuzzy protrusions of the Phe–Phe is associated with molecular conformational changes during the STM image process. (d) Combination of nanopatterning and controlled metal–organic assembly to process prestructured metallic templates. Following self-organized growth of Fe nanoarrays on the reconstructed Au(111) surface (upper left), mesoscopic organization of metallosupramolecular Fe–terephthalate ribbons is achieved by controlling the reaction conditions. Adapted from [39] ((a), (b)); [50] (c) and [51] (d).

The theoretical treatment of the interesting class of fourfold chelating ligands like porphyrins and phthalocyanines has also been performed with DFT calculations. On metal surfaces in the submonolayer regime the molecules are found to chemisorb parallel to the surface, in accordance with STM observations, with rather weak binding energies on Au or Ag substrates [10, 18, 49]. The identification of binding sites, especially for the metal center and the charge transfer between molecule and surface, provides very detailed information, not only about the spin-state and magnetic properties of the adsorbates.

The deformation and conformational changes of the molecules upon adsorption affect the hybridization of the metal d states with the surface and has consequences for the spin polarization of the coordination centers. Nevertheless, the validity of the calculation remains to be experimentally confirmed and therefore the detailed interpretation of the results on the spin polarization should be taken with care.

8. Steering accommodation of guest species and mesoscopic ordering

One of the first intentions to test the usability of the described network structures was the study of inclusion of guest molecules into the open cavities of the arrays revealing the underlying substrate. The high thermal stability and overall robustness of the structures makes them ideal templates for the (selective) adsorption of guest molecules and their templating on the surface.

The cavities of the polybenzene carboxylate networks as reported above can be controlled by the length of the backbone of the linker molecules. The cavity surrounding consists of rather inert phenyl rings, weakly interacting with other functional groups. The size of the cavities was used to steer the interaction of C_{60} molecules with the copper substrate and also the number of interacting C_{60} molecules per pore (see figure 12(a)) [39]. Furthermore, it was shown that besides the effect on the adsorbate–substrate interactions of the different

pore sizes the functionalization of the cavity rim by replacing the rod-like TPA molecule with TMLA, which possesses an additional carboxylate side group available for interactions with guest species, the effective interaction of the C_{60} with the pores and substrate can be significantly altered.

The cavities of the Fe–TMA arrays presented above, emerging from the hierarchical self-assembly of TMA molecules in the presence of Fe adatoms feature identically shaped hosts of about 1 nm, equally spaced by 3.43 nm and functionalized by eight carboxylate groups. It was successfully demonstrated that this network is capable of selective and reversible adsorption of a series of guest species, including C_{60} and small biomolecules (see figure 12(b)) [50].

There is yet another approach to patterning the surface which involves the spatial confinement of coordination reactions, e.g. by controlling the formation of clusters or the assembly of metal–organic complexes on a restricted area on the substrate. For instance, self-organized growth of Fe or Co on reconstructed Au(111) provides a means to create arrays of transition metal islands [51]. By tuning the local reaction conditions with co-deposited terephthalate linker molecules, one can follow coordination reactions [52, 45, 51] and synthesize distinct low-dimensional metallosupramolecular systems, including the regularly spaced Fe–terephthalate ribbons. With a careful tuning of the reaction conditions the corresponding gratings reflect the substrate chevron pattern, with their extension only limited by the terrace morphology which renders a mesoscopically ordered template structure (see figure 12(c)) [51].

9. Concluding remarks

The presented findings reveal that methodologies employing metal-directed assembly protocols on surfaces are promising for achieving unique low-dimensional coordination systems. They are conceivable for a great variety of systems and can be applied to substrates with different symmetries, as well as physical and chemical properties. Because of their high thermal stability the realized clusters, polymers, and networks constitute a promising route towards low-dimensional magnetism in a broad temperature range. Also the redox properties of the coordination centers present an appealing topic which needs to be further explored. Nanoporous metal–organic coordination networks can be used to arrange guest species in well-defined nanoscale environments, either for patterning purposes or for investigations of surface chemical reactions in controlled surroundings. Furthermore, they bear potential to control large biomolecules and their molecular motions in tunable spaces. Finally, they may serve as templates for the organization of separated, regularly distributed magnetic nanoclusters.

References

[1] Atwood J L, Davies J E D, MacNicol D D, Vögtle F and Lehn J-M (ed) 1996 *Comprehensive Supramolecular Chemistry* (New York: Pergamon)

[2] Lehn J-M 1995 *Supramolecular Chemistry, Concepts and Perspectives* (Weinheim: VCH)
Lawrence D S, Jiang T and Levett M 1995 *Chem. Rev.* **95** 2229
Swiegers G F and Malefetse T J 2000 *Chem. Rev.* **100** 3483
Leininger S, Olenyuk B and Stang P J 2000 *Chem. Rev.* **100** 853
Holiday B J and Mirkin C A 2002 *Angew. Chem. Int. Edn* **40** 2022

[3] Moulton B and Zaworotko M J 2001 *Chem. Rev.* **101** 1629
Yaghi O M, O'Keeffe M, Ockwig N W, Chae H K, Eddaoudi M and Kim J 2003 *Nature* **423** 705
Kitagawa S, Kitaura R and Noro S 2004 *Angew. Chem. Int. Edn* **43** 2334
Hosseini M W 2005 *Acc. Chem. Res.* **38** 313

[4] Bersuker I B 1996 *Electronic Structure and Properties of Transition Metal Compounds: Introduction to the Theory* (New York: Wiley)

[5] Gianneschi N C, Masar M S and Mirkin C A 2005 *Acc. Chem. Res.* **38** 825

[6] Badjic J D, Nelson A, Cantrill S J, Turnbull W B and Stoddart J F 2005 *Acc. Chem. Res.* **38** 723
Balzani V, Credi A, Raymo F M and Stoddart J F 2000 *Angew. Chem. Int. Edn* **39** 3348

[7] De Feyter S and De Schryver F C 2003 *Chem. Soc. Rev.* **32** 139
Barth J V, Costantini G and Kern K 2005 *Nature* **437** 671

[8] Barth J V, Weckesser J, Lin N, Dmitriev S and Kern K 2003 *Appl. Phys.* A **76** 645

[9] Barth J V 2007 *Annu. Rev. Phys. Chem.* **58** 375
Barth J V 2000 *Surf. Sci. Rep.* **40** 75
Brune H 1998 *Surf. Sci. Rep.* **31** 121
Barth J V, Weckesser J, Cai C, Günter P, Bürgi L, Jeandupeux O and Kern K 2000 *Angew. Chem. Int. Edn* **39** 1230
Barth J V, Weckesser J, Trimarchi G, Vladimirova M, De Vita A, Cai C, Brune H, Günter P and Kern K 2002 *J. Am. Chem. Soc.* **124** 7991
Weckesser J, Barth J V and Kern K 1999 *J. Chem. Phys.* **110** 5351–4
Schunack M, Linderoth T R, Rosei F, Laegsgaard E, Stensgaard I and Besenbacher F 2002 *Phys. Rev. Lett.* **88** 156102
Otero R, Hümmelink F, Sato F, Legoas S B and Thostrup P *et al* 2004 *Nature Mater.* **3** 779

[10] Zhao A *et al* 2005 *Science* **309** 1542
Wende H *et al* 2007 *Nat. Mater.* **6** 516

[11] Iancu V, Deshpande A and Hla S-W 2006 *Nano Lett.* **6** 820

[12] Ruben M, Rojo J, Romero-Salguero F J, Uppadine L H and Lehn J-M 2004 *Angew. Chem. Int. Edn* **43** 3644
Safarowsky C, Merz L, Rang A, Broekmann P, Hermann B A and Schalley C A 2004 *Angew. Chem. Int. Edn* **43** 1291
Gong J R, Wan L J, Yuan Q H, Bai C L, Jude H and Stang P J 2005 *Proc. Natl Acad. Sci.* **102** 971

[13] Grillo S E, Tang H, Coudret C and Gauthier S 2002 *Chem. Phys. Lett.* **355** 289
Gersen H, Schaub R, Xu W, Stensgaard I, Laegsgaard E, Linderoth T R, Besenbacher F, Nazeeruddin M K and Grätzel M 2006 *Appl. Phys. Lett.* **89** 264102

[14] Shoji O, Tanaka H, Kawai T and Kobuke Y 2005 *J. Am. Chem. Soc.* **127** 8598

[15] Auwärter W, Weber-Bargioni A, Brink S, Riemann A, Schiffrin A, Ruben M and Barth J V 2007 *ChemPhysChem* **8** 250

[16] Shubina T E, Marbach H, Flechtner K, Kretschmann A, Jux N, Buchner F, Steinrück H-P, Clark T and Gottfried J M 2007 *J. Am. Chem. Soc.* **129** 9476

[17] Lu X, Hipps K W, Wang X D and Mazur U 1996 *J. Am. Chem. Soc.* **118** 7190
Hipps K W, Scudiero L, Barlow D E and Cooke M P 2002 *J. Am. Chem. Soc.* **124** 2126–7
Bonifazi D, Spillmann H, Kiebele A, Wild M d, Seiler P, Cheng F, Güntherodt H-J, Jung T and Diederich F 2004 *Angew. Chem. Int. Edn* **43** 4759

Suto K, Yoshimoto S and Itaya K 2006 *Langmuir* **22** 10766
Auwärter W, Weber-Bargioni A, Schiffrin A, Riemann A, Gröning O, Fasel R and Barth J V 2006 *J. Chem. Phys.* **124** 194708
Lukasczyk T, Flechtner K, Merte L R, Jux N, Maier F, Gottfried J M and Steinrück H-P 2007 *J. Phys. Chem.* C **111** 3090
Weber-Bargioni A, Auwärter W, Klappenberger F, Reichert J, Lefrançois S, Strunskus T, Wöll C, Schiffrin A, Pennec Y and Barth J V 2008 *ChemPhysChem* **9** 89
Yoshimoto S and Itaya K 2007 *J. Porph. Phtaloc.* **11** 313
Jung T A, Schlittler R R and Gimzewski J K 1997 *Nature* **386** 696–8
Yokoyama T, Yokoyama S, Kamikado T and Mashiko S 2001 *J. Chem. Phys.* **115** 3814–8
[18] Leung K, Rempe S B, Schultz P A, Sproviero E M, Batista V S, Chandross M E and Medforth C J 2006 *J. Am. Chem. Soc.* **128** 3659
[19] Auwärter W, Klappenberger F, Weber-Bargioni A, Schiffrin A, Strunskus T, Wöll C, Pennec Y, Riemann A and Barth J V 2007 *J. Am. Chem. Soc.* **129** 11279
[20] Ruben M, Lehn J-M and Müller P 2006 *Chem. Soc. Rev.* **35** 1056
[21] Frederick B G, Leibsle F M, Haq S and Richardson N V 1996 *Surf. Rev. Lett.* **409** 512
Perry C C, Haq S, Frederick B G and Richardson N V 1998 *Surf. Sci.* **409** 512
Chen Q, Perry C C, Frederick B G, Murray P W, Haq S and Richardson N V 2000 *Surf. Sci.* **446** 63
[22] Giessen M 2001 *Prog. Surf. Sci.* **68** 1
[23] Pascual J I, Barth J V, Ceballos G, Trimarchi G, De Vita A, Kern K and Rust H-P 2004 *J. Chem. Phys.* **120** 11367
[24] Lin N, Dmitriev A, Weckesser J, Barth J V and Kern K 2002 *Angew. Chem. Int. Edn* **41** 4779
[25] Lin N, Payer D, Dmitriev A, Strunskus T, Wöll C, Barth J V and Kern K 2005 *Angew. Chem. Int. Edn* **44** 1488
[26] Dmitriev A, Lin N, Weckesser J, Barth J V and Kern K 2002 *J. Phys. Chem.* B **106** 6907
[27] Payer D, Comisso A, Dmitriev A, Strunskus T, Lin N, Wöll C, DeVita A, Barth J V and Kern K 2007 *Chem. Eur. J.* **13** 3900
[28] Messina P, Dmitriev A, Lin N, Spillmann H, Abel M, Barth J V and Kern K 2002 *J. Am. Chem. Soc.* **124** 14000
[29] Spillmann H, Dmitriev A, Lin N, Messina P, Barth J V and Kern K 2003 *J. Am. Chem. Soc.* **125** 10725
[30] Newkome G R *et al* 2006 *Science* **312** 1782
[31] Lingenfelder M, Spillmann H, Dmitriev A, Stepanow S, Lin N, Barth J V and Kern K 2004 *Chem. Eur. J.* **10** 1913
[32] Stepanow S, Strunskus T, Lingenfelder M, Dmitriev A, Spillmann H, Lin N, Barth J V, Wöll C and Kern K 2004 *J. Phys. Chem.* B **108** 19392
[33] Stepanow S, Lin N, Vidal F, Landa A, Ruben M, Barth J V and Kern K 2005 *Nano Lett.* **5** 901
Vidal F, Delvigne E, Stepanow S, Lin N, Barth J V and Kern K 2005 *J. Am. Chem. Soc.* **127** 10101
[34] Meot-Ner (Mautner) M 2005 *Chem. Rev.* **105** 213
[35] Dmitriev A, Spillmann H, Lingenfelder M, Lin N, Barth J V and Kern K 2004 *Langmuir* **41** 4799
[36] Dmitriev A, Spillmann H, Lin N, Barth J V and Kern K 2003 *Angew. Chem. Int. Edn* **41** 2670
[37] Classen T, Fratesi G, Costantini G, Fabris S, Stadler F L, Kim C, Gironcoli S d, Baroni S and Kern K 2005 *Angew. Chem. Int. Edn* **44** 6142
[38] Tait S L, Langner A, Lin N, Stepanow S, Rajadurai C, Ruben M and Kern K 2007 *J. Phys. Chem.* C **111** 10982
[39] Stepanow S, Lingenfelder M, Dmitriev A, Spillmann H, Delvigne E, Lin N, Deng X, Cai C, Barth J V and Kern K 2004 *Nat. Mater.* **3** 229
[40] Stepanow S, Lin N, Barth J V and Kern K 2006 *J. Phys. Chem.* B **110** 23472
[41] Lin N, Stepanow S, Vidal F, Kern K, Alam M S, Strömsdörfer S, Dremov V, Müller P, Landa A and Ruben M 2006 *Dalton Trans.* **2006** 2794
[42] Lin N, Stepanow S, Vidal F, Barth J V and Kern K 2005 *Chem. Commun.* 1681
[43] Stepanow S, Lin N, Payer D, Schlickum U, Klappenberger F, Zoppellaro G, Ruben M, Brune H, Barth J V and Kern K 2007 *Angew. Chem. Int. Edn* **46** 710
Schlickum U, Decker R, Klappenberger F, Zoppellaro G, Klyatskaya S, Ruben M, Silanes I, Arnau A, Kern K, Brune H and Barth J V 2007 *Nano Lett.* **7** 3813
[44] Hooks D E, Fritz T and Ward M D 2001 *Adv. Mater.* **13** 227
[45] Clair S, Pons S, Fabris S, Baroni S, Brune H, Kern K and Barth J V 2006 *J. Phys. Chem.* B **110** 5627
[46] Tait S L, Wang Y, Lin N, Costantini G, Baraldi A, Esch F, Petaccia L, Lizzit S and Kern K 2007 *J. Am. Chem. Soc.* **130** 2108–13
[47] Seitsonen A P, Lingenfelder M, Spillmann H, Dmitriev A, Stepanow S, Lin N, Kern K and Barth J V 2006 *J. Am. Chem. Soc.* **126** 5634
[48] Gambardella P *et al* 2007 submitted
[49] Zotti L A, Teobaldi G, Hofer W A, Auwärter W, Weber-Bargioni A and Barth J V 2007 *Surf. Sci.* **601** 2409
[50] Stepanow S, Lin N, Barth J V and Kern K 2006 *Chem. Commun.* 2153
[51] Clair S, Pons S, Brune H, Kern K and Barth J V 2005 *Angew. Chem. Int. Edn* **44** 7294
Barth J V, Brune H, Ertl G and Behm R J 1990 *Phys. Rev.* B **42** 9307
[52] Mendez J, Caillard R, Otero G, Nicoara N and Martin-Gago J 2006 *Adv. Mater.* **18** 2048
Grant A G, Jones T E and Baddeley C J 2007 *J. Phys. Chem.* C **111** 10534